

SCIENTIFIC REPORTS



OPEN

Bessel beams with spatial oscillating polarization

Shiyao Fu, Shikun Zhang & Chunqing Gao

Received: 08 April 2016
 Accepted: 08 July 2016
 Published: 04 August 2016

Bessel beams are widely used in optical metrology mainly because of their large Rayleigh range (focal length). Radial/azimuthal polarization of such beams is of interest in the fields of material processing, plasma absorption or communication. In this paper an experimental set-up is presented, which generates a Bessel-type vector beam with a spatial polarization, oscillating along the optical axis, when propagating in free space. A first holographic axicon (HA) HA1 produces a normal, linearly polarized Bessel beam, which by a second HA2 is converted into the spatial oscillating polarized beam. The theory is briefly discussed, the set-up and the experimental results are presented in detail.

Beams with a transverse homogeneous polarization, such as linearly, elliptically, or circularly polarized beams, are widely used in optics. In contrast to homogeneously polarized beams (circular, linear), vector vortex beams have a transversely varying polarization¹, which can be described by the higher-order Poincaré sphere^{2,3}, are attracting more and more attention for their unique characteristics. The two typical examples of vector beams are the radial or azimuthal polarization. Usually, these fields are eigen solutions of the vectorial Helmholtz equation and remain constant when propagating in free space. The transformation of the polarization states of vector beams requires wave plates, which increases the complexity of the set-up. In this paper a new kind of vector beams is presented named oscillating polarized (OP) vector beams. When propagating the polarization state is varying periodically with an oscillation length z_i determined by the two holographic axicons. The theory is briefly discussed, and an approach how to realize these beams experimentally is presented for different polarization orders. This simple set-up will be of interest for many applications, which require spatial polarization control.

The discovery of vector beams changed the understanding of polarization considerably, and has led to an improvement of optical systems. For instance, higher absorption of a vector beam contributes to their application in laser plasma heating⁴, and radial polarized vector beams have favorable focusing property⁵. In addition, vector beams are also used in fields such as optical communications^{6–8}, particle trapping^{9,10}, surface plasma excitation¹¹, image encryption¹² and so on. In contrast to homogeneously polarized beams, vector beams have a unique spatial polarization structure. The field of such a beam reads:

$$\vec{E}(\varphi, r) = A(r) \cdot \begin{bmatrix} \cos(l\varphi + \varphi_0) \\ \sin(l\varphi + \varphi_0) \end{bmatrix} \quad (1)$$

In Eq. (1), $A(r)$ is the amplitude distribution, φ the azimuthal angle, φ_0 the initial orientation of the field vector for $\varphi = 0$. l denotes the polarization order of the vector beam, also known as the topological charge of a vortex beam. Eq. (1) also represents a linearly polarized beam for $l = 0$ particularly. The state of polarization of a vector beam depends on the value of φ_0 . For instance, in the case of $l = 1$, $\varphi_0 = 0$ is the radial polarization state and $\varphi_0 = \pi/2$ is the azimuthal polarization state.

Vector beams can be generated by very different methods as inserting mode-selection elements in the laser resonator^{13–15}, transformation from optical vortices outside the resonator^{16–22} and so on. However, the polarization state of vector beams stays constant along the optical axis and can't be changed unless a wave plate is inserted in the optical path. The methods mentioned above may bring limitations for the application of vector beams. For example, in laser manufacturing, radially polarized beams are used for laser cutting²³ and azimuthal polarized beams for punching²⁴. If a vector beam contains these two polarization states in different propagation distance, the cutting and punching can be realized simultaneously. Moreno *et al.* have introduced an approach to generate nondiffracting Bessel beams with varying polarization states when propagating²⁵. Nonetheless, the polarization in different positions of the optical axis is homogeneous.

School of Opto-Electronics, Beijing Institute of Technology, Beijing 100081, China. Correspondence and requests for materials should be addressed to C.G. (email: gao@bit.edu.cn)

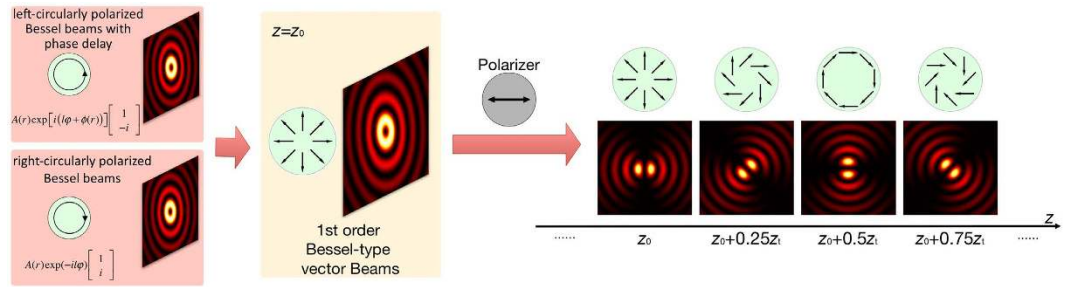


Figure 1. Schematic set-up to generate OP beams. The key idea is to introduce different additional phase-shifts at different positions of the axis. Then the state of polarization is varying with the propagation distance.

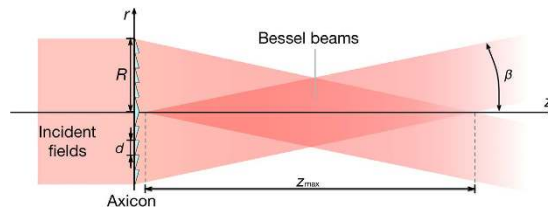


Figure 2. Axicons or axicon-holograms can be used to generate Bessel beams in the overlap region.

In this paper, by using axicon holograms realized by spatial light modulators (SLM 1, SLM 2), a new method is presented to generate Bessel-type vector beams with spatial oscillating polarization along the z -axis. The state of polarization at different positions was measured with a polarizer. The experimental results fit well the theory.

Results

Principles of generating OP vector beams. Bessel beams, solutions of Helmholtz equation in cylindrical coordinates, are widely known as a non-diffraction or self-reconstructing light beam, which can reconstruct its electric field after passing through an obstruction^{26–29}. Researches have done a lot in studying Bessel beams, and found their existence for atoms³⁰ and electron waves^{31–33}. The amplitude of a Bessel beam reads with Eq. (2):

$$E(\varphi, r) = E_0 J_l(k_r r) \exp(i l \varphi) \tag{2}$$

where J_l is the l -th order Bessel function, k_r is the radial wavenumber and l is the topological charge^{26,34,35}. The term $\exp(i l \varphi)$ also means that the Bessel beam represents an optical vortex, which carries orbital angular momentum (OAM)³⁶.

As a kind of Bessel-type vector beams^{37–40}, OP vector beams can be generated from Bessel modes. Right and left circularly polarized Bessel beams, which have opposite topological charge can be combined and result in a Bessel-type vector beam, as shown in Eq. (3)

$$\frac{1}{2} \exp(i l \varphi) \begin{bmatrix} 1 \\ -i \end{bmatrix} + \frac{1}{2} \exp(-i l \varphi) \begin{bmatrix} 1 \\ i \end{bmatrix} = \begin{bmatrix} \cos l \varphi \\ \sin l \varphi \end{bmatrix} \tag{3}$$

In Eq. (3), once an additional phase $\phi(r)$ is introduced in the left-circularly polarized component, and meanwhile it doesn't change the phase of the right-circularly polarized state. Then Eq. (3) can be written as:

$$\frac{1}{2} \exp[i(l\varphi + \phi(r))] \begin{bmatrix} 1 \\ -i \end{bmatrix} + \frac{1}{2} \exp(-i l \varphi) \begin{bmatrix} 1 \\ i \end{bmatrix} = \exp\left[\frac{1}{2} i \phi(r)\right] \begin{bmatrix} \cos\left(l\varphi + \frac{1}{2} \phi(r)\right) \\ \sin\left(l\varphi + \frac{1}{2} \phi(r)\right) \end{bmatrix} \tag{4}$$

The introduction of $\phi(r)$ in the left-circularly polarized Bessel beam leads to a change of the initial polarization. For example, in the case of $l=1$, the spatial polarization state will be changed from radial to azimuthal, when $\phi(r)$ varies between 0 and π . This effect can be used to generate OP vector beams as shown in Fig. 1.

Various additional phase shifts in different propagation distances are generated by a special holographic axicon. An axicon is a tapered optical element with circular symmetry. Figure 2 illustrates the generation of Bessel beams by an axicon. When a plane wavefront passes an axicon, it will be transformed into a conical wave. In the overlap region Bessel-like waves are generated⁴¹. The maximum range of the Bessel beams is given by the length z_{max} of this region and reads²⁵:

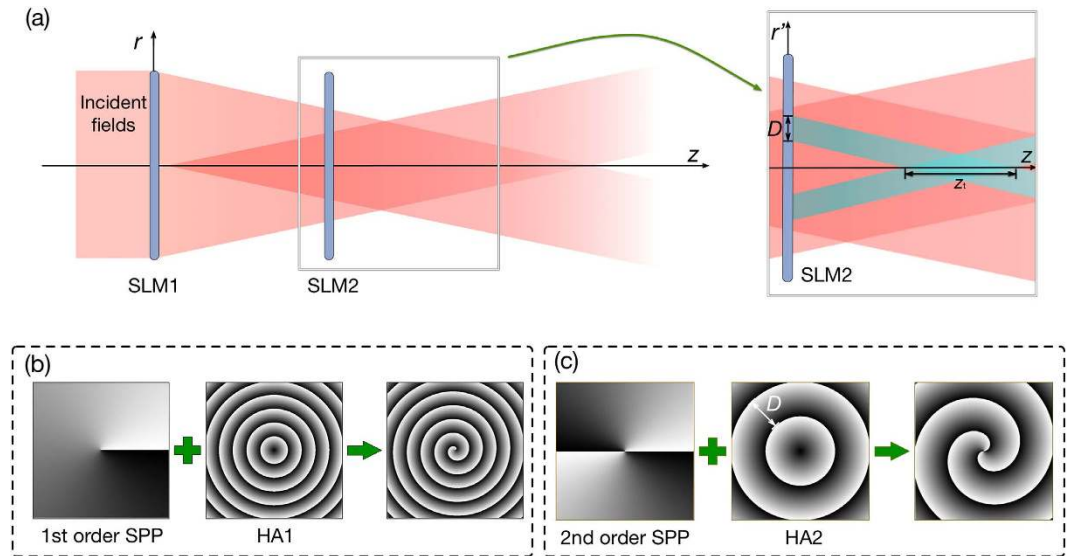


Figure 3. Two holographic axicons can introduce additional phase shifts along the optical path. (a) Scheme of realizing the additional phase in different propagation distance. SLM1 upload the combined hologram in (b) and SLM2 upload the combined hologram in (c). (b,c) show the hologram to generate first order OP vector beams. (b) The hologram on SLM1 to generate Bessel beams, which corresponds to an axicon (HA1) and a first order spiral phase plate (SPP). (c) The hologram on SLM2 to generate the additional phase shift, where HA2 combined with a second order SPP.

$$z_{\max} = \frac{Rd}{\lambda} = R \cot \beta \tag{5}$$

with λ the wavelength, R the radius of the axicon. If the beam size is smaller than the axicon’s base, R denotes the radius of the incident field. β is the refraction angle and d is the radial period of the axicon. If the incident field is horizontal linearly polarized, the Bessel beams will have the same polarization. In this experiment the axicon is replaced by a holographic axicon (HA) HA1, which can be uploaded on SLM, to generate linearly polarized Bessel beams. Now another holographic axicon HA2 with different period D is inserted and produces an additional phase shift depending now on the propagation distance z as shown in Fig. 3. Circularly polarized beams with different phase delay at different positions z are obtained after propagating through a 45° arranged quarter wave plate (QWP). The HA2’s phase distribution $\phi(r)$ is given by:

$$\phi(r) = \frac{2\pi r}{D} \tag{6}$$

with D the period of the HA2. Eq. (5) with Eq. (6) results in

$$\phi(z) = \frac{2\pi\lambda z}{Dd} \tag{7}$$

This is the additional phase shift of the propagating beam, which produces the oscillating states of polarization. The distance z_t between two equal states of polarization requires $\phi(z_t) = 2\pi$ and delivers:

$$z_t = \frac{dD}{\lambda} \tag{8}$$

The overlap region of the additional phase shift must be smaller than the Bessel beam region which requires $z_{\max} > z_t$ or $D < R$.

Experimental Setup. The experimental setup for generating OP vector beams is shown in Fig.4. The fundamental Gaussian mode with a wavelength of 1550 nm is generated by a laser diode (LD) and coupled into a single mode fiber. The Gaussian output beam is collimated (Col.) with a diameter of 3 mm and polarized linearly horizontal by a beam splitter (PBS). Only for this polarization a pure phase modulation by the SLM is possible. The beam expander (BE), a concave lens $f = -50$ mm and a convex lens $f = 100$ mm, enlarge the diameter to 6 mm.

The SLMs’ diffraction efficiency is 80%, nominal resolution 1920×1080 pixels, active area 15.36 mm \times 8.64 mm and the pixel pitch $8.0 \mu\text{m}$ (Holoeye, PLUTO-TELCO-013-C). Utilizing the performance of the polarization control⁴² and the phase modulation of SLM, we can use two SLMs to accomplish all the calculation process discussed in section 2. For generating Bessel beams, we upload the hologram of an axicon (HA1) combined with l -th order spiral phase plate (SPP), which is shown in Fig. 3(b), on SLM1. The generated

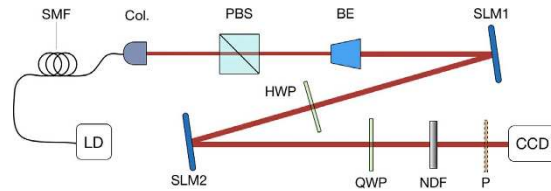


Figure 4. Experimental setup for generating OP vector beams. LD, laser diode. SMF, single mode fiber. Col., collimator. PBS, polarizing beam splitter. BE, beam expander. SLM1 and SLM2, liquid crystal spatial light modulators. HWP, half wave plate. QWP, quarter wave plate. NDF, neutral density filter. P, polarizer. CCD, infrared CCD camera.

horizontal linearly polarized Bessel beam is of $-l$ -th order, because of the reflective SLM 1. The reflection added by SLM1 contributes to the opposite topological charge. The half wave plate (HWP) is placed at an angle of 22.5° to the horizontal plane in order to rotate the polarization orientation of the Bessel beam at 45° . Thus, the generated Bessel beam has two linearly polarized components with equal intensity, a horizontal and a vertical one. After reflected by SLM2, only the horizontal polarization component will be modulated, due to the polarization feature of the SLM 1. The hologram uploaded on SLM2 consists of HA2 and a $2l$ -th order SPP, which introduces an additional phase $\phi(r)$ of the horizontal linearly polarized Bessel beam, as shown in Fig. 3(c). The topological charge of the horizontal component of the Bessel beam incident on SLM2 can be expressed as $-(-l + 2l) = -l$, which means it will not be changed. The topological charge of the vertical component will be opposite, for it is reflected by SLM2 once and is not modulated. Therefore, the light reflected by SLM2 consists of a horizontal and a vertical linearly polarized Bessel beam with opposite topological charges. The horizontal polarized component has a phase delay. A 45° quarter-wave plate (QWP) is used to transform the two combined linearly polarized Bessel beams into left and right circularly polarized helical beams. Eq. (4) is satisfied and an OP vector beam is generated.

A rotated polarizer is used to check the polarization distribution of the OP vector beam. An infrared CCD camera with the spectral range of $900\text{ nm} \sim 1700\text{ nm}$ is used for the detection.

As previously mentioned, the pixel pitch of the SLMs is $8.0\ \mu\text{m}$. For this reason, the radial period of the HA1 d and the period of the HA2 D should be set as multiples of 8 when designing the hologram shown in Fig. 5. Only by this way each liquid crystal of the SLM can be well encoded. The period of the HA1 was $880\ \mu\text{m}$, and the period of HA2 was $2184\ \mu\text{m}$. Then the spatial period of the polarization becomes with Eq. (8) $z_t = 1.24\text{ m}$.

The radius of the incident beam with $R = 3\text{ mm}$ is smaller than the axicon's base and Eq. (5) delivers for the maximum range $z_{\text{max}} = 1.70\text{ m}$. The distance between SLM1 and SLM2 is 0.43 m , the free moving range for the CCD camera behind SLM2 is 1.27 m .

Experimental results. Figure 5 summarizes the experimental and simulated results of 1st and 2nd order OP vector beams. One can see that the experimental pattern fit well with theory. The intensity distribution of the l -th order beam is similar to a Bessel beam whose topological charge is $\pm l$. The patterns are divided into $2l$ main lobes after passing through a polarizer. In the same location, for instance, $z = z_0$, the lobes will rotate at an angle of θ/l when the polarizer rotates at an angle of θ . The absence of the side lobes in some of the patterns is caused by the lower transmittance of the NDF, to make the main lobes more clearly. The unique characteristic of the OP beams is the linear rotation of the polarization distribution along the optical axis. When moving the CCD camera along the axis over a distance of $0.25z_t$, the lobes will rotate by an angle of $\pi/(4l)$, which can be explained by Eq. (7) and Eq. (4). Eq. (7) can be written as:

$$\phi(z) = \frac{2\pi z}{z_t} \quad (9)$$

which delivers $\phi = \pi/2$ if $z = 0.25z_t$. It is clear from Eq. (3) that the rotation angle of the patterns behind a polarizer is $\phi/2l$. Hence, the rotation angle of $\pi/(4l)$ is obtained.

In order to verify quantitatively this variation, the rotation angle was measured along the z -axis with a moving CCD-camera. In the measurement, the polarizer is placed at the angle of 0° . In this case, the rotation angle θ should be a linear function of the camera's position, which can be written as:

$$\theta = \frac{\phi(z)}{2l} = \frac{\pi z}{lz_t} \quad (10)$$

The pattern were measured in steps of $\Delta z = 0.05\text{ m}$. After the image processing of each pattern, the corresponding relationship between the rotation angle and CCD's position is obtained. The measurement was performed for the 1st order and the 2nd order OP vector beams. The results are shown in Fig. 6 and confirm well the theoretical considerations.

Discussion

In this paper, we demonstrate experimentally and theoretically a new kind of Bessel beams (OP vector beams) with spatial oscillating, only by applying a polarization control phase-plates. In the experiment, two different

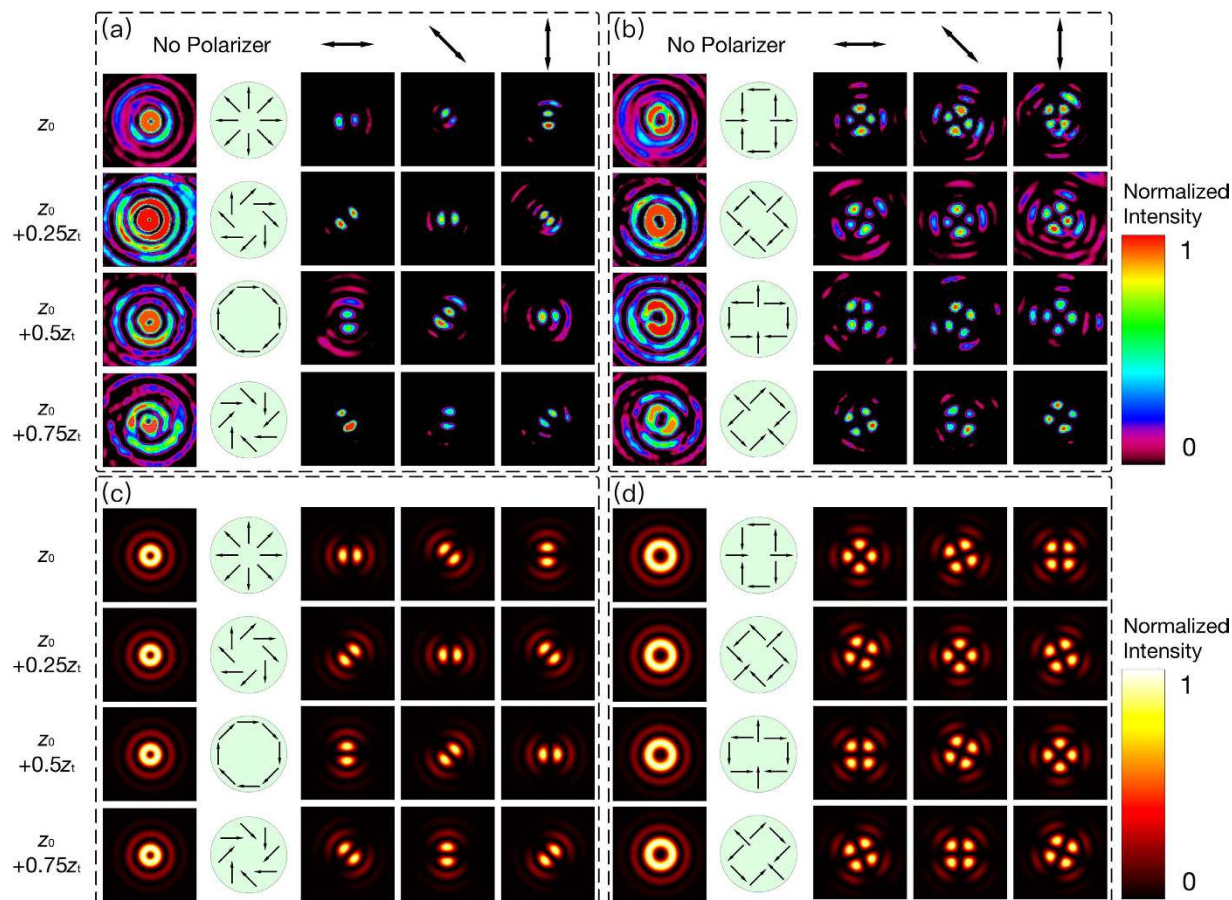


Figure 5. Experimental and simulated results of generating 1st and 2nd order OP vector beams. (a) Experimental 1st order OP vector beams. (b) Experimental 2nd order OP vector beams. (c) Simulated 1st order OP vector beams. (d) Simulated 2nd order OP vector beams. From left to right, the observed patterns without and with polarizer at 0°, 45°, 90°, respectively. From top to bottom, the patterns observed by CCD camera at different positions on the optical axis. The green areas show the spatial distribution of the polarization at different positions.

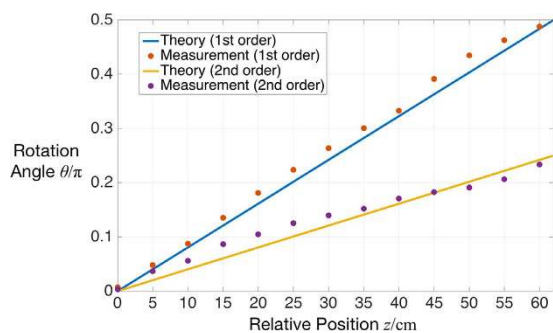


Figure 6. The angle of rotation vs the z -position for 1st and 2nd order OP vector beams behind a 0°-polarizer.

holograms are uploaded on the two SLMs. The 1st and the 2nd order OP-vector beams were generated in the experiment. In addition, the linear variation of the spatial polarization when propagating is illustrated.

The OP vector beams exist in the Bessel overlap region only, which is also called the nondiffraction zone. It can be extended by enlarging the radial period of the axicon (HA1). Another important feature of OP vector beams is the spatial variation period, which is related to the radial period of HA1 and HA2, and the wavelength of the incident beams. Arbitrary variation periods can be designed by proper choice of the parameters.

Methods

Measurement of the rotation angle. In order to verify the rotation angle of the patterns, the center of gravity of each lobe in the optical fields has to be measured. It is given by the first intensity moment⁴³:

$$\begin{cases} \bar{x}_m = \frac{1}{P} \iint_{\infty} xG(x, y) dx dy \\ \bar{y}_m = \frac{1}{P} \iint_{\infty} yG(x, y) dx dy \end{cases} \quad (11)$$

where $G(x, y) \in [0, 1]$ is the normalized gray level in the position (x, y) . P is the sum of all local gray levels:

$$P = \iint_{\infty} G(x, y) dx dy \quad (12)$$

There are two lobes in the case of 1st order OP-vector beams. Therefore, the rotation angle can be calculated by:

$$\theta = \arctan \left(\left| \frac{\bar{y}_2 - \bar{y}_1}{\bar{x}_2 - \bar{x}_1} \right| \right) \quad (13)$$

As for the 2nd order OP vector beams, two of the four lobes in the diagonal were analyzed. The rotation angle is given by:

$$\theta = \arctan \left(\left| \frac{\bar{y}_3 - \bar{y}_1}{\bar{x}_3 - \bar{x}_1} \right| \right) \quad (14)$$

References

- Zhan, Q. Cylindrical vector beams: from mathematical concepts to applications. *Advances in Optics and Photonics*. **1**, 1–57 (2009).
- Milione, G., Sztul, H. I., Nolan, D. A. & Alfano, R. R. Higher-Order Poincaré Sphere, Stokes Parameters, and the Angular Momentum of Light. *Physical Review Letters*. **107**, 053601 (2011).
- Holleczek, A., Aiello, A., Gabriel, C., Marquardt, C. & Leuchs, G. Classical and quantum properties of cylindrically polarized states of light. *Optics Express*. **19**, 9714–9736 (2011).
- Zhan, Q. Evanescent Bessel beam generation via surface plasmon resonance excitation by a radially polarized beam. *Opt. Lett.* **31**, 1726–1728 (2006).
- Quabis, S., Dorn, R., Eberler, M., Glockl, O. & Leuchs, G. Focusing light to a tighter spot. *Optics Communications*. **179**, 1–7 (2000).
- Kim, W. C., Park, N. C., Yoon, Y. J., Choi, H. & Park, Y. P. Investigation of Near-Field Imaging Characteristics of Radial Polarization for Application to Optical Data Storage. *Optical Review*. **14**, 236–242 (2007).
- Cheng, W., Haus, J. W. & Zhan, Q. Propagation of vector vortex beams through a turbulent atmosphere. *Opt. Express*. **17**, 17829–17836 (2009).
- Zhao, Y. & Wang, J. High-base vector beam encoding/decoding for visible-light communications. *Opt. Lett.* **40**, 4843–4846 (2015).
- Kozawa, Y. & Sato, S. Optical trapping of micrometer-sized dielectric particles by cylindrical vector beams. *Opt. Express*. **18**, 10828–10833 (2010).
- Tian, B. & Pu, J. Tight focusing of a double-ring-shaped, azimuthally polarized beam. *Opt. Lett.* **36**, 2014–2016 (2011).
- Zhou, Z., Tan, Q. & Jin, G. Surface plasmon interference formed by tightly focused higher polarization order axially symmetric polarized beams. *Chin. Opt. Lett.* **8**, 1178–1181 (2010).
- Li, X., Lan, T. H., Tien, C. H. & Gu, M. Three-dimensional orientation-unlimited polarization encryption by a single optically configured vectorial beam. *Nature Communications* **3**, 998 (2012).
- Li, J., Ueda, K., Musha, M., Zhong, L. & Shirakawa, A. Radially polarized and pulsed output from passively Q-switched Nd:YAG ceramic microchip laser. *Opt. Lett.* **33**, 2686–2688 (2008).
- Enderli, F. & Feurer, T. Radially polarized mode-locked Bd:YAG laser. *Opt. Lett.* **34**, 2030–2032 (2009).
- Iwahashi, S. *et al.* Higher-order vector beams produced by photonic-crystal lasers. *Opt. Express*. **19**, 11963–11968 (2011).
- Wang, X. L., Ding, J., Ni, W. J., Guo, C. S. & Wang, H. T. Generation of arbitrary vector beams with a spatial light modulator and a common path interferometric arrangement. *Opt. Lett.* **32**, 3549–3551 (2007).
- Maurer, C., Jesacher, A., Furfapter, S., Bernet, S. & Ritsch-Marte, M. Tailoring of arbitrary optical vector beams. *New Journal of Physics*. **9**, 78 (2007).
- Jones, P. H., Rashid, M., Makita, M. & Marago, O. M. Sagnac interferometer method for synthesis of fractional polarization vortices. *Opt. Lett.* **34**, 2560–2562 (2009).
- Xin, J. *et al.* Generation and detection of linearly polarized axially symmetric beam by an amplitude computer-generated hologram. *Optics Communication*. **285**, 3688–3691 (2012).
- Xin, J., Gao, C., Li, C. & Wang, Z. Generation of polarization vortices with a Wollaston prism and an interferometric arrangement. *Appl. Opt.* **51**, 7094–7097 (2012).
- Liu, S., Li, P., Peng, T. & Zhao, J. Generation of arbitrary spatially variant polarization beams with a trapezoid Sagnac interferometer. *Opt. Express*. **20**, 21715–21721 (2012).
- Fu, S. *et al.* Generating polarization vortices by using helical beams and a Twyman Green interferometer. *Opt. Lett.* **40**, 1775–1778 (2015).
- Niziev, V. G. & Nesterov, A. V. Influence of beam polarization on laser efficiency. *Journal of Physics D* **32**, 1455–1461 (1999).
- Meier, M., Romano, V. & Feurer, T. Material processing with pulsed radially and azimuthally polarized laser radiation. *Applied Physics A* **86**, 329–334 (2007).
- Moreno, I., Davis, J. A., Sánchez-López, M. M., Badham, K. & Cottrell, D. M. Nondiffracting Bessel beams with polarization state that varies with propagation distance. *Opt. Lett.* **40**, 5451–5454 (2015).
- Durnin, J. Exact solutions for nondiffracting beams. I. The scalar theory. *J. Opt. Soc. Am. A* **4**, 651–654 (1987).
- Aiello, A. & Woerdman, J. P. Goos-Hänchen and Imbert-Fedorov shifts of a nondiffracting Bessel beam. *Optics Letters*. **36**, 543–545 (2011).
- Ornigotti, M. & Aiello, A. Generalized Bessel beams with two indices. *Optics Letter*. **39**, 5618–5621 (2014).
- Aiello, A. & Agarwal, G. S. Wave-optics description of self-healing mechanism in Bessel beams. *Optics Letters*. **39**, 6819–6822 (2014).

30. Hayrapetyan, A. G., Matula, O., Surzhykov, A. & Fritzsche, S. Bessel beams of two-level atoms driven by a linearly polarized laser field. *The European Physical Journal D*. **67**, 167 (2013).
31. Grillo, V., Karimi, E., Gazzadi, G. C., Frabboni, S., Dennis, M. R. & Boyd, R. W. Generation of Nondiffracting Electron Bessel Beams. *Physical Review X*. **4**, 011013 (2014).
32. Bliokh, K. Y., Dennis, M. R. & Nori, F. Relativistic Electron Vortex Beams: Angular Momentum and Spin-Orbit Interaction. *Physical Review Letters*. **107**, 174802 (2011).
33. Hayrapetyan, A. G., Matula, O., Aiello, A., Surzhykov, A. & Fritzsche, S. Interaction of Relativistic Electron-Vortex Beams with Few-Cycle Laser Pulses. *Physical Review Letters*. **112**, 134801 (2014).
34. Durnin, J., Miceli, J. J. & Eberly, J. H. Diffraction-free beams. *Phys. Rev. Lett.* **58**, 1499–1501 (1987).
35. Gatto, A., Tacca, M., Martelli, P., Boffi, P. & Martinelli, M. Free-space orbital angular momentum division multiplexing with Bessel beams. *Journal of Optics* **13**, 064018 (2011).
36. Allen, L., Beijersbergen, M. W., Spreeuw, R. J. C. & Woerdman, J. P. Orbital angular momentum of light and the transformation of Laguerre-Gaussian laser modes. *Phys. Rev. A*. **45**, 8185–8189 (1992).
37. Madhi, D., Ornigotti, M. & Aiello, A. Cylindrically polarized Bessel-Gauss beams. *Journal of Optics*. **17**, 025603 (2015).
38. Ornigotti, M. & Aiello, A. The Hertz vector revisited: a simple physical picture. *Journal of Optics*. **16**, 105705 (2014).
39. Ornigotti, M. & Aiello, A. Radially and azimuthally polarized nonparaxial Bessel beams made simple. *Optics Express*. **21**, 15530–15537 (2013).
40. Bouchal, Z. & Olivik, M. Non-diffractive Vector Bessel Beams. *Journal of Modern Optics*. **42**, 1555–1566 (1995).
41. Scott, G. & Mcardle, N. Efficient generation of nearly diffraction-free beams using an axicon. *Optical Engineering* **31**, 2640–2643 (1992).
42. Moreno, I., Davis, J. A., Hernandez, T. M., Cottrell, D. M. & Sand, D. Complete polarization control of light from a liquid crystal spatial light modulator. *Opt. Express* **20**, 364–376 (2012).
43. Hodgson, N. & Weber H. Laser Resonators and Beam Propagation, *Springer Series in Optical Sciences* 108, NY (2005).

Acknowledgements

The authors acknowledge Prof. Horst Weber of Technical University of Berlin for the helpful discussion. This work is supported by the National Basic Research Program of China (973 Program) under contract of No. 2014CB340002 and No. 2014CB340004.

Author Contributions

S.F. conceived the original idea. S.F. and C.G. completed the theoretical analysis and the simulation. S.F. and S.Z. carried out the experiments. All authors analyzed the experimental results and contribute to the writing and reviewing of this paper.

Additional Information

Competing financial interests: The authors declare no competing financial interests.

How to cite this article: Fu, S. *et al.* Bessel beams with spatial oscillating polarization. *Sci. Rep.* **6**, 30765; doi: 10.1038/srep30765 (2016).



This work is licensed under a Creative Commons Attribution 4.0 International License. The images or other third party material in this article are included in the article's Creative Commons license, unless indicated otherwise in the credit line; if the material is not included under the Creative Commons license, users will need to obtain permission from the license holder to reproduce the material. To view a copy of this license, visit <http://creativecommons.org/licenses/by/4.0/>

© The Author(s) 2016